Plasmonics
https://doi.org/10.1007/s11468-024-02210-x

RESEARCH

Wave-Guided Surface Plasmonic Resonance Induced Giant and Tunable Photonic Spin Hall Effect with Polarization Mode Control

Monu Nath Baitha[1] · Yeonhong Kim[1] · Heoung-Jae Chun[1] · Kyoungsik Kim[1]

Received: 20 December 2023 / Accepted: 23 January 2024

Abstract
The photonic spin Hall effect (PSHE) at the optical interface is a polarization-dependent phenomenon of incident light. The described methodology is a novel strategy for controlling the active polarization mode of the enhanced PSHE. The PSHE is enhanced for both horizontal (*H*) and vertical (*V*) polarized light in the ~ 1.5 mm to the submillimeter range. The enhanced PSHE has been measured for the reflected light from the modified Kretschmann configuration. An additional thin dielectric (glass) layer on the ultrathin metal (Ag, Al) layer provides simultaneous surface plasmon resonance (SPR) and wave-guiding effects. Furthermore, we demonstrated that by changing the physical parameter of the structure, we could tune the enhancement of PSHE along with the control on polarization mode. This research paves the way for new photonic devices with ultra-high sensitivity for metrological applications. Furthermore, depending on the light spin, this work enables a degree of freedom in the choosing of input light polarization for numerous potential applications.

Keywords Photonic spin Hall effect (PSHE) · Surface plasmonic resonance (SPR) · Wave-guiding (WG) effect · Modified Kretschmann configuration · Ultrathin metal layer

Introduction

The photonic spin Hall effect (PSHE) refers to the light spin accumulation in the opposite direction to each other [1]. The PSHE occurs when a linearly polarized light splits into two photonic spins left-handed circularly polarized (LCP) and right-handed circularly polarized (RCP) components, along a route perpendicular to the gradient of refractive indexes (RI) [1, 2]. The conservation of angular momentum of light, in other words, spin–orbit interaction (SOI) is the basic optical phenomenon of light and also the underlying cause behind the PSHE [3]. The incident light interaction with anisotropic or spatially inhomogeneous materials results in spin–orbit angular momentum coupling, which is responsible for several amazing phenomena as the light's angular momentum conversion, PSHE, and plasmonic vortex [4]. The SOI, which designates the coupling between orbital and spin angular momentums of light beams, has recently attracted a lot of attention. Due to its physical significance in contemporary optics, it has potential applications in a wide range of fields, including precision metrology [5], spin-photonics [6], topological photonics [7], and quantum optical networks [8]. Because of the inherently weak SOI, the PSHE normally occurs in a few nanometers range and also depends on the incident polarization.

A related phenomenon, known as the Imbert–Fedorov shift in total internal reflection of light, was theoretically predicted in 1955 [9] and experimentally observed in 1972 [10]. Onoda et al. originally introduced the PSHE idea theoretically [11], and Hosten and Kwiat successfully validated it for an air-glass contact [8]. Following this, studies on the PSHE have expanded to cover topological [7] and chiral materials [12], metallic [13] and magnetic [14] thin films, two-dimensional materials [15], metamaterials [16] and metasurface [17], and photonic crystals [18] (PhCs). These investigations have focused mostly on exploring the PSHE behavior with different systems. To enhance the naturally weak PSHE, a variety of nanophotonic approaches have been studied, including the near Brewster angle [19], surface plasmon resonance (SPR) [20, 21], multilayer thin film [22], and

Monu Nath Baitha and Yeonhong Kim equally contributed to this work.

✉ Kyoungsik Kim
kks@yonsei.ac.kr

[1] School of Mechanical Engineering, Yonsei University, 50 Yonsei-ro, Seodaemun-gu, Seoul 03722, Republic of Korea

long-range SPR [23]. These approaches have been employed to develop extremely sensitive RI sensors [24], image edge detection [25], optical switches and filters [26], biosensors [27], and metrology applications [5] based on the PSHE effect. However, the degree of PSHE enhancement in many of the identified structures related to SPR is still limited to H-polarized only, which restricts its widespread use across several fields [21]. As the PSHE is a dependent function on incident polarization and angle, one of the recent studies by Kim et al. showed an isotropic and anisotropic interface mechanism to achieve polarization-independent PSHE at an angle as well as for all incident angles [28, 29]. Simultaneously, in a separate study by Baitha and Kim, polarization-independent PSHE for all incident angles has been presented with all isotropic interfaces [30]. Control over the polarization dependency of PSHE may lead to advancement in the development of practical devices.

In this study, we investigate the idea of enhancing the PSHE by altering the conventional Krestmann design. The waveguiding and SPR effects are evident simultaneously due to the added glass layer on a thin metal (Ag/Al) layer. We have observed that the enhancement in PSHE, as described in previously reported plasmonic platform-based enhancement in PSHE, is only confined to H-polarized $\left(\delta_{\pm}^{H}\right)$ [21]. On the other hand, this work enables the regulated encasement of PSHE for both H and V-polarized modes. This research is expanded to look at the enhanced giant PSHE in many ways in terms of different metal layers and physical alterations of the structure such as thickness. We highlight the strategy to control the predominant polarization-enhanced PSHE with tenability. The important findings described here are to develop a better understanding of how to design future applications with control over light spin accumulation.

Geometry

The schematic representation of PSHE by a plan polarized incident wave of 632.8-nm wavelength $\left(\lambda_0\right)$ through an optical interface is shown in Fig. 1a. The incident and reflected waves are each associated with a set of Cartesian coordinates $\left(x_i, y_i, z_i\right)$ and $\left(x_r, y_r, z_r\right)$, respectively. A similar phenomenon of PSHE with light spin separation $\delta_r^{\pm}$ is shown for the adopted geometry in Fig. 1b. A thin metal (Ag/Al) layer of thickness $\left(t_1\right)$ and RI $\left(n_1\right)$ is at the base of the glass prism. An additional thin glass layer of thickness $\left(t_2\right)$ and RI $\left(n_2\right)$ is sandwiched between the thin metal layer and air substrate. To compute the presented study, the RI of Ag $\left(n_1^{Ag}\right)$ and Al $\left(n_1^{Al}\right)$ are taken as $0.0589+4.2430i$ and $1.3763+7.6165i$, respectively [30]. The RI of the glass prism (n_0) and thin glass waveguiding layer (n_2) is the same at 1.515. The study has been carried out for two different thicknesses, 1 nm and 5 nm, of the metal layer and the thickness of the waveguiding layer has been calibrated to achieve the maximum enhanced giant PSHE.

Compared to a standard Kretschmann configuration composed of prism-metal-air layers, here, an additional thin glass sandwiched between metal and air proved a waveguided-SPR (Fig. 1c). In the conventional structure, the electromagnetic (EM) field of SPR is generated at the metal-air interface only

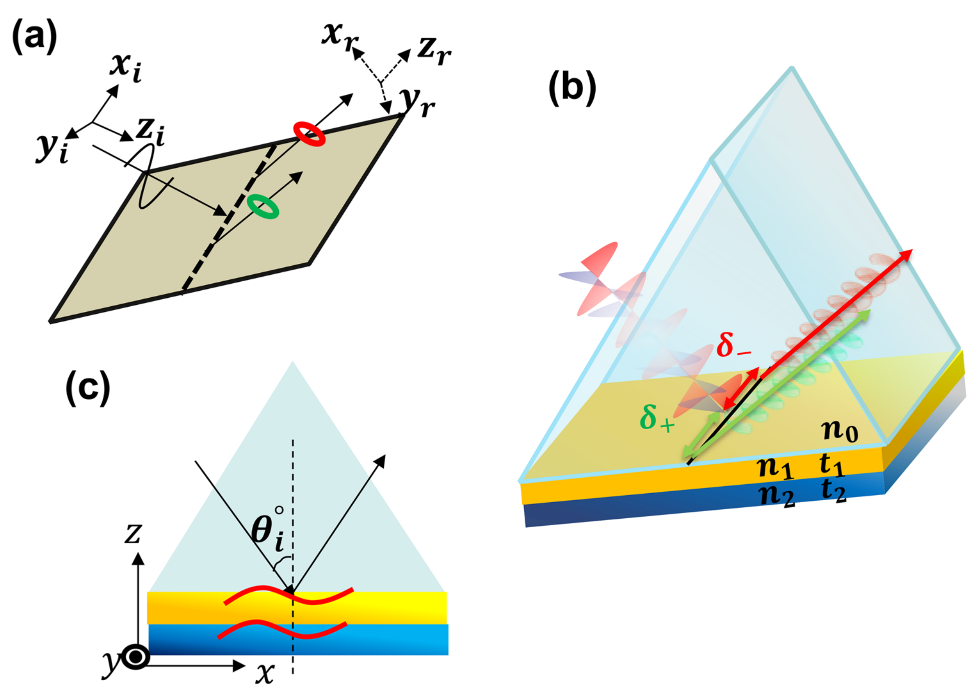

Fig. 1 **a** Schematic diagram of the general scheme of optical Hall effect of the reflected light from an interface. **b** Adopted modified Kretschmann configuration, where ultrathin metal sandwiched between a prism and additional dielectric (wave-guiding) layer **c** Generated surface wave propagation at both interface of the ultrathin metal layer

[31]. In contrast to that, the proposed geometry provides two metal interface prism-metal-glasses in the proposed modified geometry. The EM field generated at these interfaces starts to interact and as a result forms symmetric and anti-symmetric EM fields at the interface. The symmetric EM field penetrates more into the glass layer as compared to the anti-symmetry EM field, and it is called long-range SPR while the anti-symmetry is named short-range SPR [32]. The appearance of long-range SPR becomes the key factor behind the enhancement of giant PSHE to the order of 10^6 nm, shown in detail in the next section.

The previously published study served as the basis for the PSHE formulation [30]. At the macroscale, the behavior of light reflected or refracted from an optical contact is described by the Fresnel equation and Snell's law. This falls under the category of incident light being considered as a single wave vector. Microscopically, however, this is not the case. The incident wave is made up of the central wave vector k_{zi} and the non-zero, non-centered wave vectors k_{xi} and k_{yi}.

As per the spin basis system, the angular spectrum may be represented as $E_i^H = \left(E_{i+} + E_{i-}\right)/\sqrt{2}$ and $E_i^V = i\left(E_{i-} - E_{i+}\right)/\sqrt{2}$. The horizontal and vertical polarization states of light are represented here by the superscripts H and V, respectively. The LCP and RCP wave components are indicated using the subscripts positive (+) and negative (−), respectively. The formulation pertains to a monochromatic Gaussian beam exhibiting an extremely narrow spectrum:

$$E_{i,r} = \frac{\omega_0}{\sqrt{2\pi}} \exp\left(-\frac{\omega_0^2\left(k_x^2 + k_y^2\right)}{4}\right) \tag{1}$$

where ω_0 is the beam waist. The relationship between the reflected light in terms of incident light is given as follows.

The beam waist is represented by ω_0 here. The relationship between reflected light and the incident light is stated as:

$$\begin{bmatrix} E_r^H \\ E_r^V \end{bmatrix} = \begin{bmatrix} r_p & \frac{k_{ry}\cot\theta_i(r_p+r_s)}{k_0} \\ -\frac{k_{ry}\cot\theta_i(r_p+r_s)}{k_0} & r_s \end{bmatrix} \begin{bmatrix} E_i^H \\ E_i^V \end{bmatrix} \tag{2}$$

r_p and r_s are the Fresnel reflection coefficient for p- and s-polarized incident waves. The transfer matrix method (TMM) [33] was used in this work to determine the variables r_p and r_s. k_0 is used to indicate the free space wave number. By considering Eqs. (1) and (2), the relation for reflected angular spectrum is given as:

$$\mathrm{E}_\mathrm{r}^\mathrm{H} = \frac{r_p}{\sqrt{2}}\left[e^{(ik_{ry}\delta_{r+}^{H})}E_{r+} + e^{(-ik_{ry}\delta_{r-}^{H})}\mathrm{E}_{r-}\right] \tag{3}$$

$$E_\mathrm{r}^\mathrm{V} = i\frac{r_s}{\sqrt{2}}\left[-e^{(ik_{ry}\delta_{r+}^{V})}E_{r+} + e^{(-ik_{ry}\delta_{r-}^{V})}E_{r-}\right] \tag{4}$$

$e^{(\pm ik_{ry}\delta_r^{H,V})}$, term describing the SOI of light [20]. The final expression for the PSHE of reflected light of H and V polarized light is:

$$\delta_{r\pm}^{H} = \mp\frac{\lambda_0}{2\pi}\left[1 + \frac{|r_s|}{|r_p|}\cos(\varphi_s - \varphi_p)\right]\cot\theta_i \tag{5}$$

$$\delta_{r\pm}^{V} = \mp\frac{\lambda_0}{2\pi}\left[1 + \frac{|r_p|}{|r_s|}\cos(\varphi_p - \varphi_s)\right]\cot\theta_i \tag{6}$$

where $\delta_{r\pm}^{H}$ and $\delta_{r\pm}^{V}$ are the PSHE for horizontal and vertical polarized light wave; θ_i and λ_0 are the incident angle and wavelength of light. For both s- and p-polarized incident light, the phase shift of light after reflection is shown as φ_s and φ_p, respectively.

Result and Discussion

PSHE from Kretschmann Configuration

A conventional Kretschmann configuration contains a metal layer, positioned on the bottom of the prism, which is the most often used technique for producing SPR [34]. In the current work, the ultrathin metal layers of Ag and Al with thicknesses of 1 and 5 nm have been taken into consideration. Figure 2a to d show the calculated H- and V-polarized PSHE components $\left(\delta_+^{H,V}\right)$. In comparison to the 5-nm layer, the PSHE $\left(\delta_+^{H,V}\right)$ is larger for the 1-nm-ultrathin layer because the thinner metal layer provides the more significant plasmonic behavior [35]. Figure 2e to h display the Fresnel reflection coefficients (FRC) $\left|r_{s,p}\right|/\left|r_{p,s}\right|$ ratio. The high magnitude PSHE (Fig. 2a–d) is made possible by a larger FRC ratio (Fig. 2e–g). Figure 2i to l depict the Fresnel reflection coefficient for an ultrathin (1 and 5 nm) metal (Ag and Al) layer for p- and s-plane polarized incident waves. The maximum amount of reflection occurs at an angle of about ~ 45° (Fig. 2i–l), which appears due to the total internal reflection of the light wave from glass to air. The dips in $\left|r_p\right|$ are caused by the surface plasmon resonance effect (Fig. 2i–l). Because plasmonic resonance cannot occur with an s-polarized incident wave, there are no dips in $\left|r_s\right|$ (Fig. 2i–l). As SPR is only created by p-polarized waves, the $\left|r_p\right|$, $\left|r_s\right|/\left|r_p\right|$ and δ_+^H are more dominant in all cases than their counterparts $\left|r_s\right|$, $\left|r_p\right|/\left|r_s\right|$ and δ_+^V. This observation is in agreement with the earlier documented PSHE for thin Ag nanolayers [13].

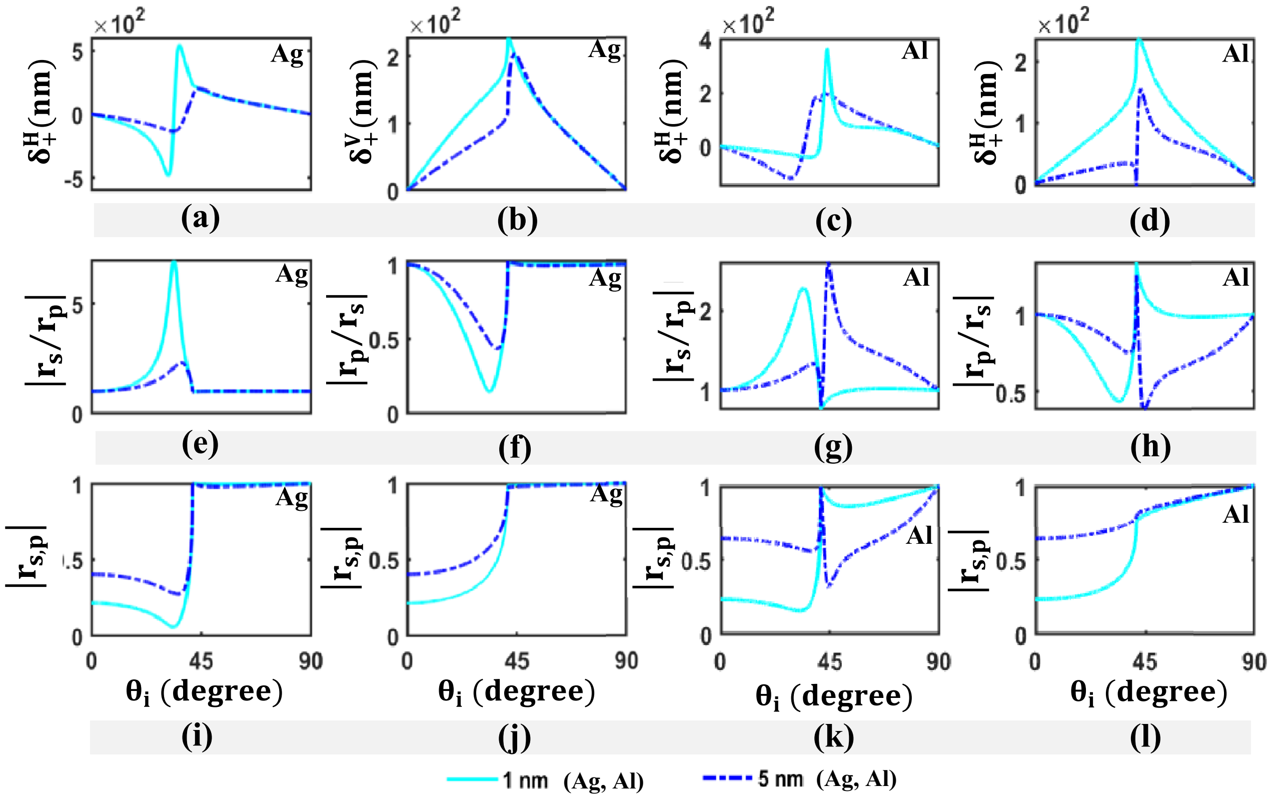

Fig. 2 Photonic spin Hall effect (**a–d**), absolute Fresnel reflection coefficient ratio (**e–h**), and Fresnel reflection coefficient (**i–l**) for standard Kretschmann configuration with Ag/Al metal layer of 1-nm (solid) and 5-nm (dotted) thickness

PSHE with an Additional WG Layer on Ag

In this study, we propose the SPR structures with a wave-guiding layer, WG-SPR. Two different thin metal layers (Ag and Al) are utilized, and Fig. 3 describes the calculations of PSHE and Fresnel reflection coefficient ratio of the WG-SPR model with a thin Ag layer. The thickness of the WG thin glass layer (t_2) is optimized, while the Ag layer (t_1) is maintained at a constant thickness of 1 nm. The variations of δ_+^V and δ_+^H relative to the angle of incidence are explained in Fig. 3a–d. At a wave-guiding layer thickness of 61.3 nm, the resonance condition is fulfilled at an angle of incidence $(\theta_i = 30.4°)$. The H-polarized enhanced PSHE, δ_+^H measures $\sim 2.7 \times 10^5$ nm (Fig. 3a) at this resonance condition, whereas the δ_+^V is insignificantly smaller than the δ_+^H.

The incident light undergoes a slight modification in polarization bases and accumulates a spin-dependent geometric phase as it is traveling transversely $(k \cdot E = 0)$, giving rise to the PSHE phenomenon. Following Eq. (5), the lateral displacement or PSHE observed in reflected light, resulting from an incident horizontally polarized (H-polarization) wave, denoted as δ_+^H is directly linked to the $|r_s|/|r_p|$ ratio. Notably, when the $|r_s|/|r_p|$ ratio is high near a resonant dip (Fig. 3e–h), there is a substantial escalation in the transverse shifts of H-polarization. Furthermore, as demonstrated by Eq. (6), the enhancement in transverse shifts for V-polarization relies on the high $|r_p|/|r_s|$ ratio in proximity to the resonant dip. The achievement of a nearly zero $|r_s|$ value significantly augments the $|r_p|/|r_s|$ ratio, thereby leading to the realization of an enhanced PSHE, δ_+^V.

As illustrated in Fig. 3, the substantial enhancement of PSHE is closely linked to a notably high $|r_s|/|r_p|$ ratio, which attains a value of approximately $\sim 3.4 \times 10^3$ (Fig. 3e). The impact of the angle of incidence and physical parameters on SPR generation is well recognized. By conducting a parameter analysis on the thickness of the WG layer (t_2) to optimize it based on resonance conditions, insights helped to understand how the thin glass WG layer influences the primary polarization mode and resonance angle.

The subsequent resonance condition emerges at an incidence angle of $\theta_i^{\circ} = 35.4°$. A wave-guiding layer thickness of 192.8 nm yields an $|r_s|/|r_p|$ ratio of approximately $\sim 8.9 \times 10^3$ (Fig. 3f), leading to an enhanced PSHE of around $\sim 1.3 \times 10^6$ nm (Fig. 3b). Further exploration involves observing responses as the thickness of the

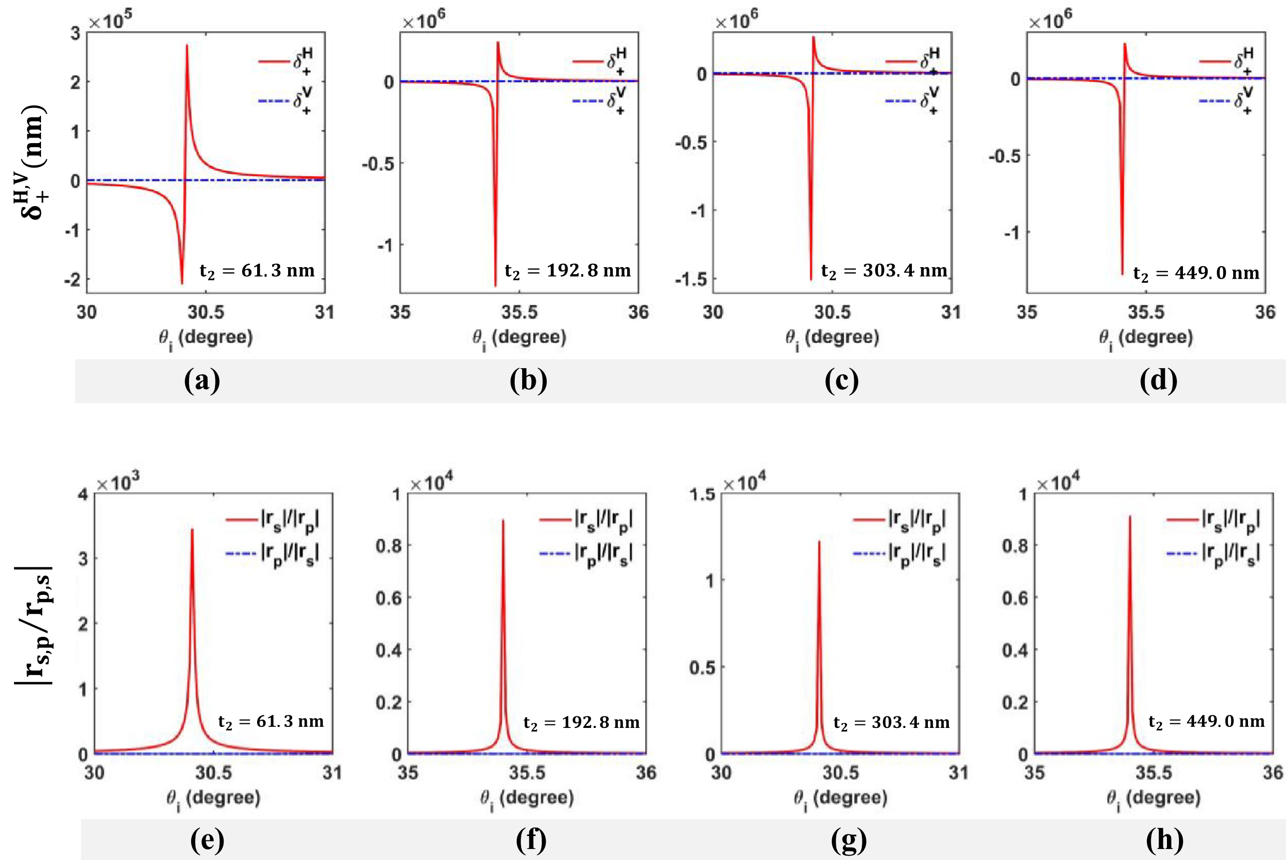

Fig. 3 The PSHE for horizontal and vertical polarizations, denoted as δ_+^H and δ_+^V, respectively, relative to the angle of incidence for a given constant thickness of Ag layer ($t_1 = 1$ nm) and varying the thicknesses of wave-guiding glass layer **a** $t_2 = 61.3$ nm, **b** $t_2 = 192.8$ nm, **c** $t_2 = 303.4$ nm, and **d** $t_2 = 449.0$ nm. Similarly, the ratios of the absolute FRC, $\left|r_{s,p}\right|/\left|r_{p,s}\right|$, relative to the angle of incidence for a given constant thickness of Ag layer ($t_1 = 1$ nm) and varying the thicknesses of wave-guiding glass layer **e** $t_2 = 61.3$ nm, **f** $t_2 = 192.8$ nm, **g** $t_2 = 303.4$ nm, and **h** $t_2 = 449.0$ nm

wave-guiding layer increases. Consequently, additional resonance conditions manifest with incident angles of 30.4° and 35.4°, corresponding to WG layer thicknesses of 303.4 nm and 449.0 nm, respectively. This pattern exhibits an alternating periodicity, as evident in Table 1. Notably, the third incident resonance angle aligns with the first resonance angle of 30.4°, while the fourth incident resonance angle corresponds to the second resonance angle of 35.4. For the polarization active mode, only *H*-polarization is observed when the thickness of Ag layer, t_1, is 1 nm. In the resonance situation, the incident wave and the guided wave of the WG layer are coupled together because one of the guided wave's propagation constants coincides with k_x. Specifically because of energy transfer into the WG layer via the Ag layer, the intensity of the reflected field is significantly reduced.

Table 1 The criteria for enhanced PSHE as the thickness of the metal (Ag) layer remains constant at 1 nm. Optimized thin glass WG layer thickness, resonance angle, and resonance polarization mode are all summarized

Thickness of dielectric cap layer (glass) (t_2 (nm))	Resonance angle (θ°)	Resonance polarization mode
61.3	30.4°	Horizontal
192.8	35.4°	Horizontal
303.4	30.4°	Horizontal
449.0	35.4°	Horizontal

With the variation of Ag layer thickness, the PSHE has been computed for further comprehension of the influence of Ag layer thickness. Figure 4 shows that the WG layer, t_2, is optimized for resonance at $t_1 = 5$ nm. The SPR behavior is found when the WG layer is 73.3 nm, leading to a nearly negligible value of $\left|r_s\right|$ at an incidence angle of 32.3°. A high $\left|r_p\right|/\left|r_s\right|$ ratio is obtained in the order of $\sim 2.8 \times 10^3$, as shown in Fig. 4e. Consequently, *V*-polarized enhanced PSHE, δ_+^V, is shown in the order of $\sim 2.2 \times 10^5$ nm (Fig. 4a).

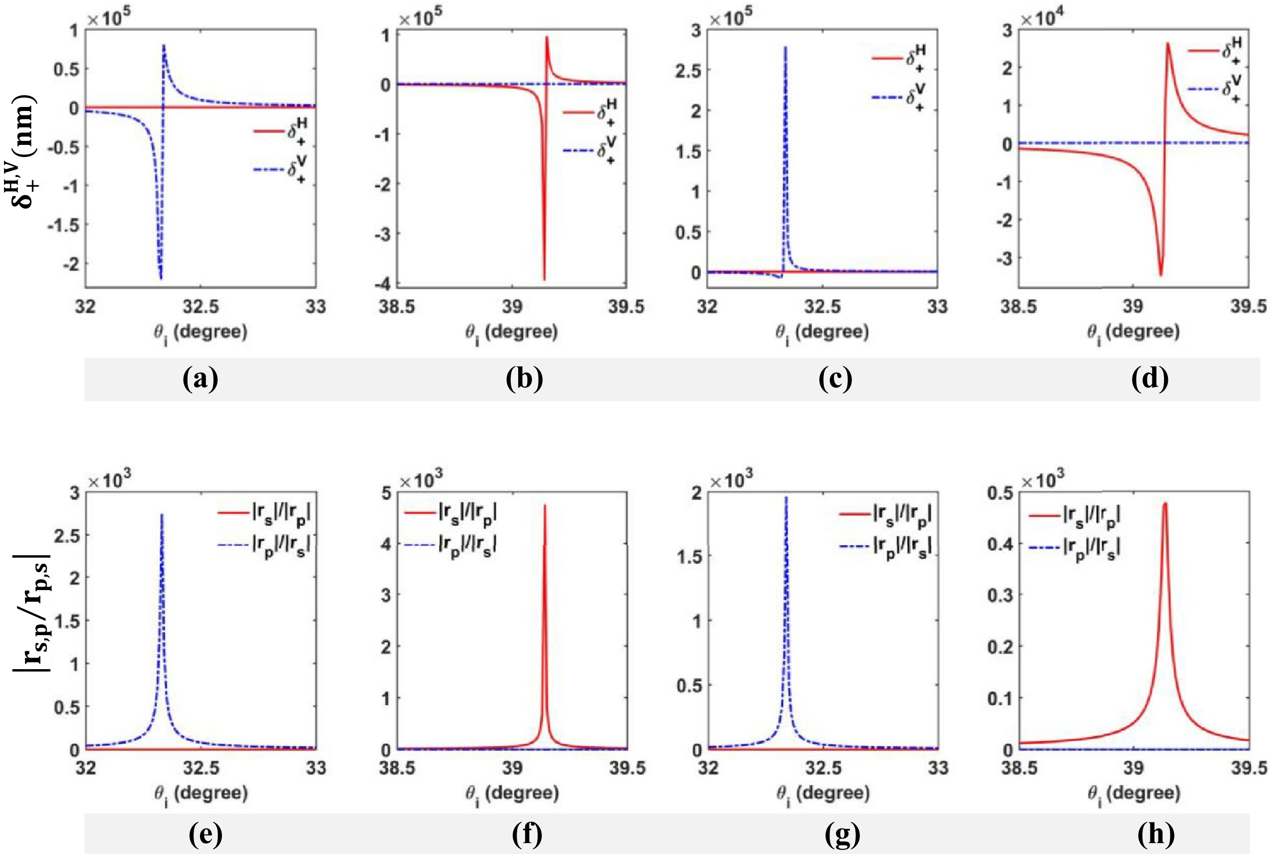

Fig. 4 The PSHE for horizontal and vertical polarizations, denoted as δ_+^H and δ_+^V, respectively, relative to the angle of incidence for a given constant thickness of Ag layer ($t_1 = 5$ nm) and varying the thicknesses of wave-guiding glass layer **a** $t_2 = 73.3$ nm, **b** $t_2 = 208.5$ nm, **c** $t_2 = 320.5$ nm, and **d** $t_2 = 477.8$ nm. Similarly, the ratios of the absolute FRC, $\left|r_{s,p}\right|/\left|r_{p,s}\right|$, relative to the angle of incidence for a given constant thickness of Ag layer ($t_1 = 1$ nm) and varying the thicknesses of wave-guiding glass layer **e** $t_2 = 73.3$ nm, **f** $t_2 = 208.5$ nm, **g** $t_2 = 320.5$ nm, and **h** $t_2 = 477.8$ nm

While setting the thickness of the Ag layer to 5 nm, the compatible glass layer thicknesses of the WG layer are carried out in further study. Next, enhanced PSHE appeared for *H*-polarized incident light. With a constant condition of the incident angle at 39.1° and the thickness of the WG layer is 208.5 nm, $\left|r_s\right|/\left|r_p\right|$ ratio appeared to be $\sim 4.7 \times 10^3$ (Fig. 4f) and *H*-polarized enhanced PSHE of $\sim 3.9 \times 10^5$ generated. Mostly, the prevailing polarization mode for PSHE has traditionally been *H*-polarization for the SPR model, as SPR arises solely from TM waves. However, the presence of guided optical waves by introducing an additional WG layer beneath the Ag layer with optimized physical parameters leads to achieving enhanced PSHE not only for TM waves but also for TE waves.

In the widely used Kretschmann configuration for local field enhancement, only incident waves with *p*-polarization at a specific resonance angle are utilized. However, prior research indicates that it is also feasible to achieve field enhancement for *s*-polarized waves at low- and high-index dielectric interfaces [36]. To achieve maximum intensity of evanescent waves, the final layer, which is air in this scenario, needs to have a low RI. By adopting this modified Kretschmann configuration, the evanescent wave is effectively enhanced for both incident waves with *s*- and *p*-polarizations. Moreover, while the thin metal layer greatly boosts the *p*-polarized evanescent wave, the dielectric layer maintains the amplification of the *s*-polarized evanescent wave and, the proposed structure, significantly enhancing the evanescent field for both *s*- and *p*-polarized waves. The importance of waveguide mode characterization, as emphasized earlier, remains pivotal.

The RI or the thickness of the layer exerts a substantial influence on the excitation of evanescent waves. In the proposed adapted Kretschmann configuration, there is a notable impact on the overall response, when altering the thickness of the WG layer. Moreover, it showcases the capability to control the primary polarization mode effectively. By pinpointing the optimal thickness for the dielectric layer, precise control over the dominant resonance mode is achievable.

Table 2 The criteria for enhanced PSHE as the thickness of the metal (Ag) layer remains constant at 5 nm. The optimized thin glass WG layer thickness, resonance angle, and resonance polarization mode are all summarized

Thickness of dielectric cap layer (glass) (t_2 (nm))	Resonance angle (θ°)	Resonance polarization mode
73.3	32.3°	Vertical
208.5	39.1°	Horizontal
320.5	32.3°	Vertical
477.8	39.1°	Horizontal

The resonance behavior of the WG-SPR with the thickness of the Ag layer (t_1 = 5nm) is summarized in Table 2, and the periodicity of the alternating pattern is observed for the desirable polarization mode and the resonance incident angle. For WG layer thickness of 73.3 and 320.5 nm, the incidence angle of 32.3° results in the dominant resonance of the vertical polarization mode, while the fourth incident resonance angle corresponds to the second resonance angle of 35.4 for horizontal polarization.

PSHE with an Additional WG Layer on Al

Aluminum has been employed as the new metallic layer, and analogous procedures to those applied with Ag have been executed. The computations based on the WG-SPR model with an Al metal layer are depicted in Fig. 5. In this analysis, the thickness of the WG layer (t_2) is optimized, while the Al layer (t_1) is maintained at a constant thickness of 1 nm. The variations in δ_+^V and δ_+^H concerning the angle of incidence are plotted in Fig. 5. At a WG layer thickness of 190.5 nm, the resonance condition is met at an incidence angle (θ_i° = 37.9°). Under this resonant circumstance, the enhanced PSHE for *H*-polarized light, δ_+^H, registers at approximately ~ 4.0 × 10^4 nm, whereas the PSHE for *V*-polarized light, δ_+^V, is comparatively negligible in comparison to δ_+^H.

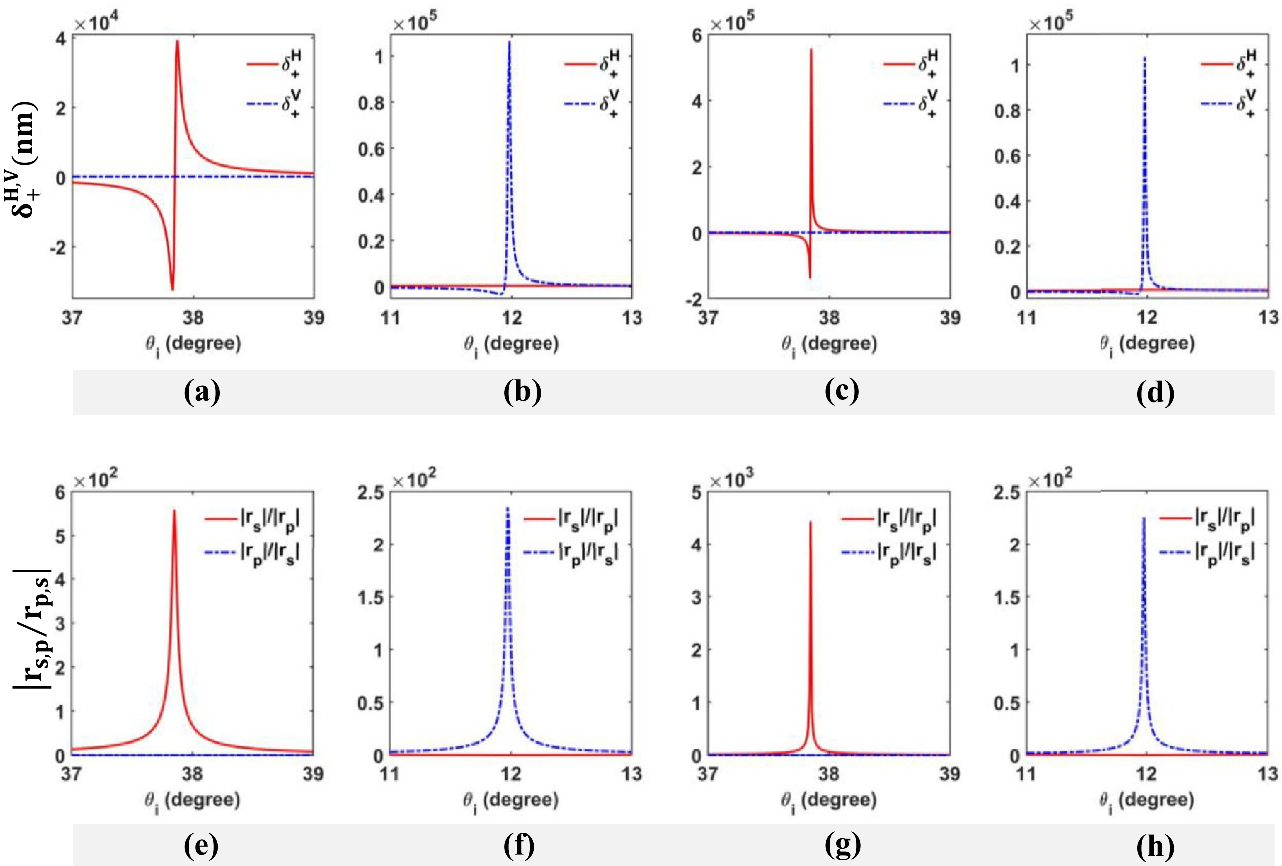

Fig. 5 The PSHE for horizontal and vertical polarizations, denoted as δ_+^H and δ_+^V, respectively, relative to the angle of incidence for a given constant thickness of Al layer (t_1 = 1 nm) and varying the thicknesses of wave-guiding glass layer **a** t_2 = 190.5 nm, **b** t_2 = 261.7 nm, **c** t_2 = 454.7 nm, and **d** t_2 = 475.2 nm. Similarly, the ratios of the absolute FRC, $\left|r_{s,p}\right|/\left|r_{p,s}\right|$, relative to the angle of incidence for a given constant thickness of Al layer (t_1 = 1 nm) and varying the thicknesses of wave-guiding glass layer **e** t_2 = 190.5 nm, **f** t_2 = 261.7 nm, **g** t_2 = 454.7 nm, and **h** t_2 = 475.2 nm

As shown in Fig. 5, the large enhanced PSHE is followed by a significant $|r_s|/|r_p|$ ratio, which is $\sim 5.6 \times 10^2$.

Through a detailed parameter analysis involving the thickness of the glass WG layer (t_2) in order to fine-tune the resonance condition, we gain insights into how the WG layer affects the primary polarization mode and resonance angle.

The next resonance condition is seen at the incidence angle ($\theta_i^\circ = 12.0°$). At a WG layer thickness of 261.7 nm with the order of $\sim 2.3 \times 10^2$ $|r_p|/|r_s|$ ratio, the enhanced PSHE is achieved in the order of $\sim 1.0 \times 10^5$. Additional investigation is done by observing the responses with the increment of the thickness of WG layer. As a result, other resonance conditions emerged with incident resonance angles of 37.9° and 12.0° at t_2 is 454.7 and 475.2 nm, orderly.

The resonance behavior of the WG-SPR with the thickness of the Al layer ($t_1 = 1$ nm) is summarized in Table 3, and the periodicity of the alternating pattern is observed for the dominant polarization mode and the resonance incident angle. For thin glass WG layer thicknesses of 190.5 and 454.7 nm, the incidence angle of 37.9° results in the dominant resonance of the horizontal polarization mode. Conversely, the vertical polarization mode is dominant resonance at the incidence angle of 12.0° for WG layer thicknesses of 261.7 and 475.2 nm.

With the variation of Al layer thickness, the PSHE has been computed for further comprehension of the influence of Al layer thickness. Figure 6 shows that the WG layer, t_2, is optimized for resonance at $t_1 = 5$ nm. SPR behavior is detected when the WG layer is 136.3 nm, leading to a nearly negligible value of $|r_s|$ at an incidence angle of 43.9°. A high $|r_p|/|r_s|$ ratio is obtained with the condition of $|r_s| < |r_p|$ at the resonance angle, as shown in Fig. 6. Consequently, V-polarized enhanced PSHE, δ_+^V, is shown in the order of $\sim 1.8 \times 10^5$ nm.

While setting the thickness of the Al layer to 5 nm, a number of various thicknesses of the WG layer are tried for further study. Another enhanced PSHE appeared for H-polarized incident light. With a constant condition of the incident angle at 41.2° and the thickness of the WG layer is 224.1 nm, $|r_s|/|r_p|$ ratio appeared to be $\sim 1.9 \times 10^2$, and an H-polarized enhanced PSHE is generated.

Table 3 The criteria for enhanced PSHE as the thickness of the metal (Al) layer remains constant at 1 nm. The optimized thin glass WG layer thickness, resonance angle, and resonance polarization mode are all summarized

Thickness of dielectric cap layer (glass) (t_2 (nm))	Resonance angle (θ°)	Resonance polarization mode
190.5	37.9°	Horizontal
261.7	12.0°	Vertical
454.7	37.9°	Horizontal
475.2	12.0°	Vertical

The resonance behavior of the WG-SPR with the thickness of the Al layer ($t_1 = 5$ nm) is summarized in Table 4, and the periodicity of the alternating pattern is observed for the active polarization mode and the resonance incident angle. For WG layer thickness of 136.3 and 426.0 nm, the incidence angle of 43.9° results in the dominant resonance of the vertical polarization mode. Conversely, the horizontal polarization mode is dominant resonance at the incidence angle of 41.2° for a WG layer thickness of 224.1 nm.

Analysis of the Effect of the WG Layer with Each Metal Layer (Al and Ag)

In this study, they proposed a novel WG-SPR structure, combining wave-guiding and surface plasmon resonance effects, modifying the conventional Kretschmann configuration. Unlike standard configurations using only p-polarized waves for SPR, this structure enhances evanescent waves in both s- and p-plane polarized incident waves [36–38]. The additional glass dielectric layer acts as a waveguide, offering the hybrid resonance modes and significantly increasing the evanescent field for both the incident polarization waves. The collective response is sensitive to layer thickness and refractive index [34]. Optimal dielectric layer thickness enables the precise control over dominant resonance mode.

The reflection coefficient vanishes for p-polarized waves ($r_p = 0$) at the dielectric interface if the angle of incidence is Brewster's angle. Consequently, there is a remarkable transformation in PSHE near the Brewster's angle, approaching its possible maximum enhanced value. At the Brewster angle, a divergence phenomenon occurs due to the p-polarized wave having a Fresnel reflection coefficient of zero. This results in a corresponding zero value for the PSHE of reflected light of V polarized light, δ_r^V (Eq. (6)). Many researchers have made some efforts to study the fundamental physics of PHSE near the Brewster angle. A modified model for PSHE with the dielectric interface under the consideration of the Brewster angle is also introduced [39]. Unlike previous studies, this work focuses on the interface between the WG layer (glass) and metal layer (Ag and Al), characterized by an RI in complex form. In this context, at the resonance angle, the ratio ($|r_{s,p}|/|r_{p,s}|$) preserves a finite value. The Brewster angle at the dielectric interface and the SPR resonance angle at metal-dialectic are often different from one another. The p-polarized SPR resonance angle does not correspond to a Brewster angle of the metal layer [31].

Investigation of the enhanced PSHE is done by employing the WG-SPR model with two different materials applying

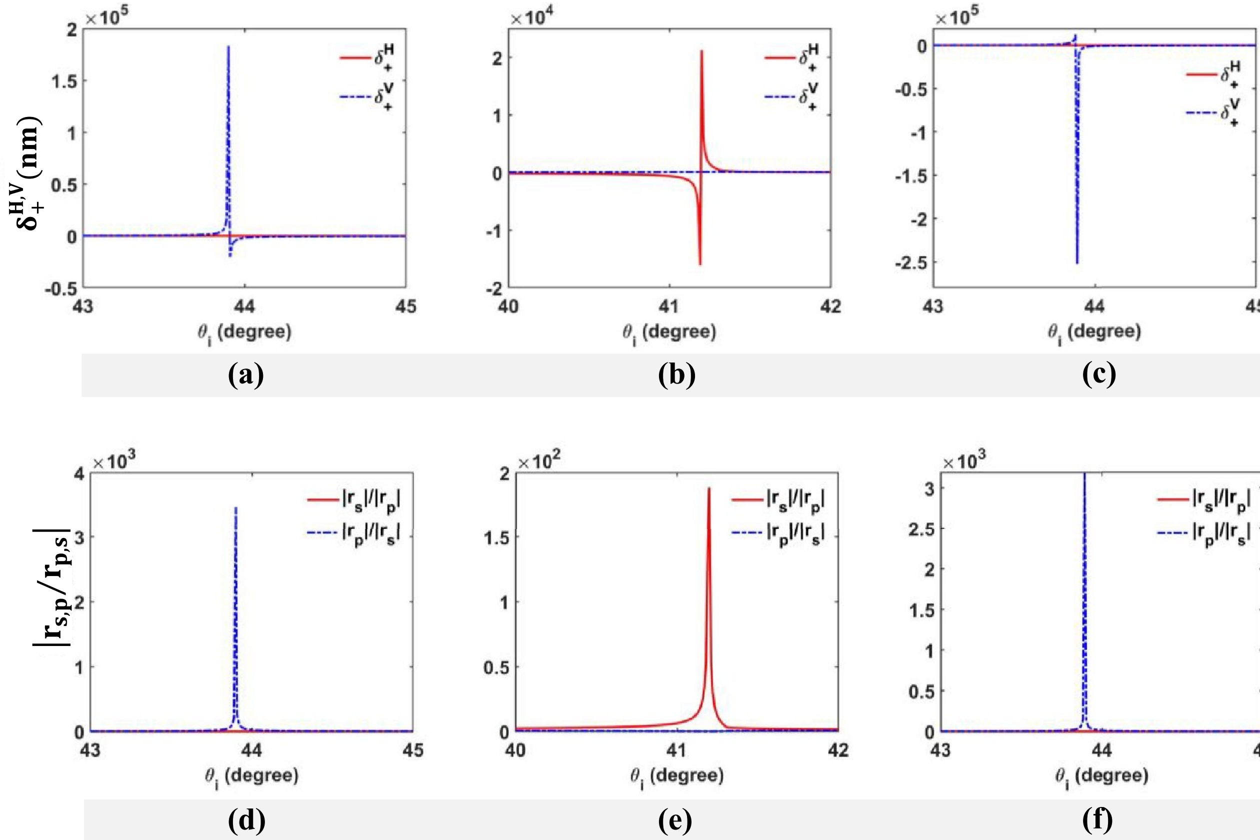

Fig. 6 The PSHE for horizontal and vertical polarizations, denoted as δ_+^H and δ_+^V, respectively, relative to the angle of incidence for a given constant thickness of Al layer ($t_1 = 5$ nm) and varying the thicknesses of wave-guiding glass layer **a** $t_2 = 136.3$ nm, **b** $t_2 = 224.1$ nm, and **c** $t_2 = 426.0$ nm. Similarly, the ratios of the absolute FRC, $|r_{s,p}|/|r_{p,s}|$, relative to the angle of incidence for a given constant thickness of Al layer ($t_1 = 5$ nm) and varying the thicknesses of wave-guiding glass layer **d** $t_2 = 136.3$ nm, **e** $t_2 = 224.1$ nm, and **f** $t_2 = 426.0$ nm

different physical parameters. Ag and Al are tested with the thickness of the metal layer, t_1, which is 1 and 5 nm, and the thickness of glass, t_2, is varied in relation to the resonance condition. By looking at Eqs. (5) and (6), we may conclude that the PSHE is influenced by the wavelength of the incident light, the Fresnel reflection coefficient (or its ratio), and the phase acquired during reflection. In our investigation, PSHE study is executed with respect to varying incident angles, while wavelength of incident light is kept constant. Furthermore, the Fresnel reflection coefficient depends on the concerned material's refractive index. In the context of the layered structure under consideration, the Fresnel reflection coefficient is governed by effective refractive index of the structure. Furthermore, any alterations introduced to the layered structure, specifically modifications in the thickness of the metal layer and/or waveguide layer, induce changes in the structure's effective refractive index. This adjustment in the effective refractive index modifies both the Fresnel reflection coefficient and the phase. Because of this, it is possible to tune the magnitude of the photonic spin Hall effect (PSHE) by different metals (Ag/Al) and thicknesses of the wave-guiding layer.

Table 4 The criteria for enhanced PSHE as the thickness of the metal (Al) layer remains constant at 5 nm. The optimized thin glass WG layer thickness, resonance angle, and resonance polarization mode are all summarized

Thickness of dielectric cap layer (glass) (t_2 (nm))	Resonance angle ($\theta°$)	Resonance polarization mode
136.3	43.9°	Vertical
224.1	41.2°	Horizontal
426.0	43.9°	Vertical

At $t_1 = 1$ nm for both Ag and Al, the maximum transverse shift occurred, and the increment in t_1 affects the decrement of PSHE. Two-dimensional ultrathin Ag film (~ nm) and Al film(~ nm) each possess high surface plasmon resonance properties [35]. The physics of photonics and plasmonic systems can be controlled when the size of the material is

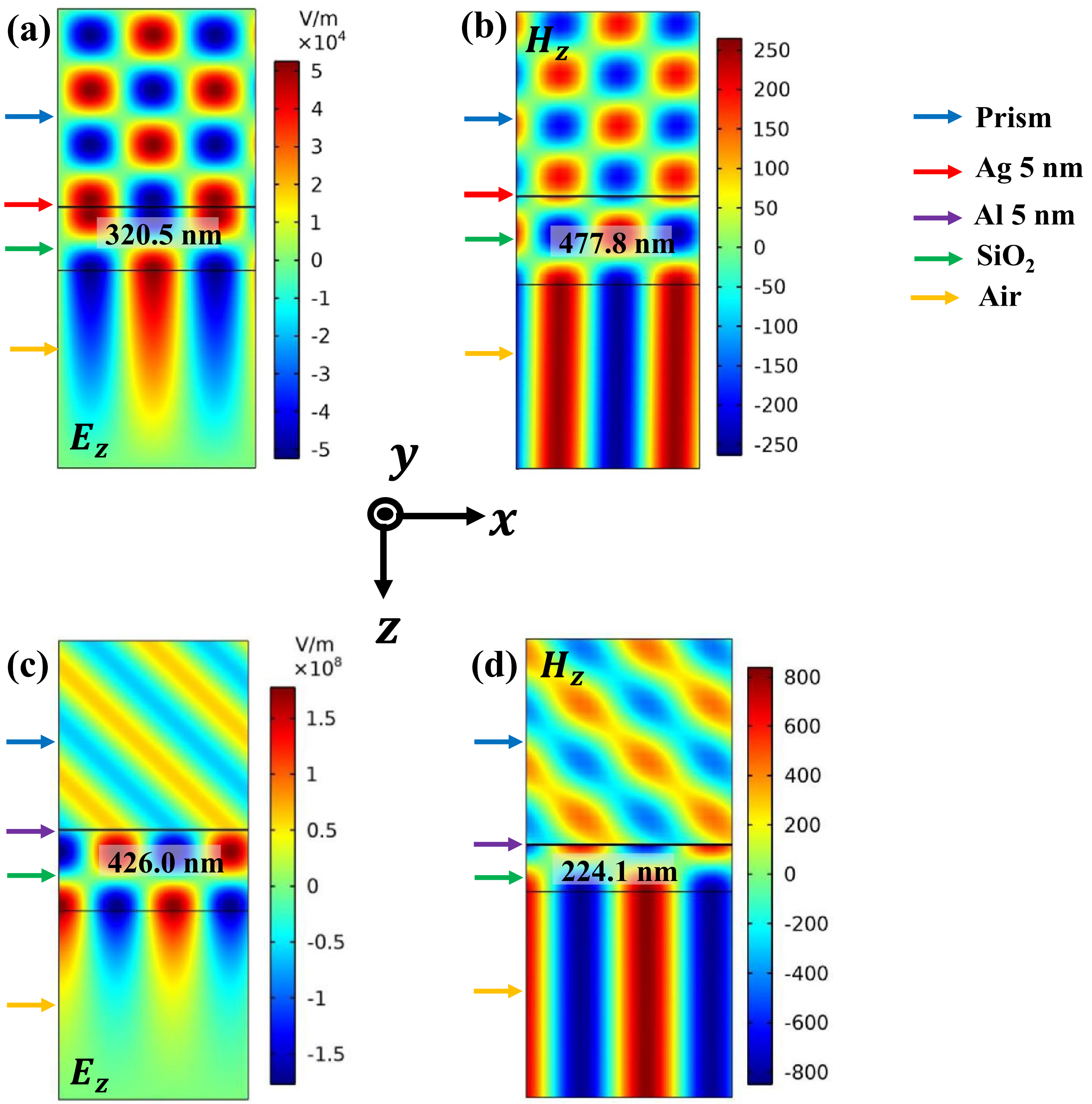

Fig. 7 Depiction of the Z-component of the electric field distribution (Ez) for TE mode and the magnetic field distribution (Hz) for TM mode under specific conditions. The thicknesses of the wave-guiding layer are **a** 320.5 nm and **b** 477.8 nm for Ag 5 nm, similarly, for Al 5 nm with wave-guiding layer thicknesses of **c** 426.0 nm and **d** 224.1 nm. This provides a visual representation of the field dynamics influenced by material composition and layer thickness

set to the nanometer scale. High SPR is generated by the surface carrier density, n_s. The bulk carrier density, denoted as n_B, significantly surpasses the surface carrier density (n_B >> n_s) [40]. These two quantities share directly proportional correlations to the thickness of the metal layer. The equation is as follows, $n_s = n_B \bullet t$, and t is equal to the thickness of the metal layer. A high n_s value for substantial plasmonic resonance can be obtained by decreasing the thickness of the metal layer to a few nanometers' scale. As in the case of graphene, the decrease in the surface plasmonic wavelength, λ_p, is offered by the few nanometers of ultrathin Ag and Al films [41]. Irrespective of the metal's material and thickness, the electric field confinement is vertically extended away from the film at a distance of ~ $\lambda_p/4\pi$. In contrast, enhancement in interaction with adjacent materials, a dielectric layer, is accomplished with the reduction in Ag and Al layer thicknesses. This observation presents a significant prospect for achieving a robust surface plasmon resonance (SPR), resulting in a considerable decrease in the reflection coefficient, approaching a value close to zero.

This work presents that the thickness of the metal layer (Ag and Al) with nanometer-scale enables the generation of two-dimensional (2-D) plasmonic. Due to their useful optical and optoelectronic properties, ultrathin Au films have been employed as the most feasible approach for plasmonic [35, 42]. The result of this study suggests that the ultrathin Ag and Al films with the correct parameters can also be a viable solution for plasmonic. Due to the limited presence of electrons in thin films, they exhibit heightened sensitivity to their environment, making them responsive to electrical gating and enabling substantial plasmonic shifts in ultrathin metal layers [42]. Fortunately, with the advancement of technology in the fabrication of nanostructures, the plasmonic response can be readily accessed these days [43]. From an experimental standpoint, achieving the deposition of metal layer films with dimensions as small as 1 nm or a few nanometers is now feasible. With the current advancements in fabrication technology, it is possible to create thin metal layer films with specific characteristics. Research conducted by Cercos et al. showcased the fabrication of gold (Au) and silver (Ag) metal layer films with subatomic thickness, approximately 1 nm, by utilizing CuO as a seed layer [44]. Another study by Maniyara et al. reported the experimental observation of tunable plasmonic behavior generated by a subatomic-thick metal layer, around 1 nm in thickness [40]. Additionally, Wang et al. demonstrated a deposition methodology for metal films with dimensions in the few nanometer range, approximately 2 nm [45]. These findings underscore the possibilities and capabilities within the realm of nanoscale metal layer film deposition, highlighting the potential for various applications in advanced materials and technologies.

Ultimately, by incorporating a WG layer into an ultrathin metal layer (Ag and Al), the active polarization mode of enhanced PSHE can be controlled. Furthermore, the resonance incidence angle can be adjusted by carefully selecting the physical dimensions of the proposed WG-SPR model.

It is a well-established fact that SPR generation exclusively occurs through TM (*H*-polarized) waves. An additional simulation study is conducted on the two-dimensional equivalent structure of the presented model (depicted in Fig. 1) using COMSOL Multiphysics to validate the resonance induced by TE (*V*-polarization) wave. The significance role of the wave-guiding layer is elucidated in Fig. 7, where simulated field profiles of incident TM and TE waves reveal strong field confinements within the wave-guiding layer and at two interfaces: one at the metal-wave-guiding layer and the other at the wave-guiding layer–air interface. These pronounced field confinements affirm the near-zero Fresnel reflection coefficients $\left|r_{s,p}\right|$ for both TE and TM waves, respectively. This observation supports the enhanced PSHE for both *H*- and *V*-polarized waves in an SPR-based model due to the induced wave-guiding-SPR effect. We aimed to demonstrate the impact of a wave-guiding layer on enhancing PSHE through polarization control, employing this COMSOL simulation study. For Ag with a thickness of 5 nm and SiO_2 with a thickness of 320.5 nm exciting TE incident waves, a resonance condition is observed, resulting in the field accumulation in wave-guiding layer that supported enhancement of *V*-polarized PSHE, as evidenced in Fig. 7a. Similarly, for TM incident waves, Fig. 7b demonstrates a comparable behavior with a SiO_2 thickness of 477.8 nm. A parallel investigation was conducted for an Al layer of 5-nm thickness, with a SiO_2 layer thickness of 426.0 nm for TE mode incident waves (Fig. 7c) and 224.1 nm for TM mode incident waves (Fig. 7d).

Conclusion

In summary, the proposed modified Kretschmann configuration has been successful in enhancing PSHE for both *H*- and *V*-polarized incident waves within a plasmonic context. The introduction of an additional glass WG layer facilitates long-range surface plasmon resonance (SPR), resulting in a high $\left|r_{s,p}\right|/\left|r_{p,s}\right|$ ratio, along with nearly zero $\left|r_{s,p}\right|$. This substantial ratio of absolute Fresnel coefficients is responsible for the considerable PSHE enhancement by around 10^6 nm, surpassing previous models [20, 46]. Furthermore, these findings demonstrate the ability to control the dominant polarization mode and tune the PSHE enhancement by manipulating the thickness of the glass layer. This research shows the potential applications in modern quantum optics, where the polarization state of both *H*- and *V*-polarized waves plays a significant role.

Author Contributions M. N. B. and Y.K. contributed equally in conceptualization, investigation, formal analysis, Writing – original draft. K. K. and H. J. C. contributed in funding acquisition, resources, supervision, validation, Writing – review & editing. All authors have read and agreed to the final version of the manuscript.

Funding This work was supported by Korea Research Institute for defense Technology planning and advancement (KRIT) grant funded by the Korea government (DAPA (Defense Acquisition Program Administration)) (No. 20–105-E00-005(KRIT-CT-23–010), VTOL Technology Research Center for Defense Applications, 2023.

Data Availability The data that supports the findings of this study is available within the article.

Declarations

Competing Interests The authors declare no competing interests.

References

1. Bliokh KY, Bliokh YP (2006) Conservation of angular momentum, transverse shift, and spin Hall effect in reflection and refraction of an electromagnetic wave packet. Phys Rev Lett 96:073903
2. Baitha MN, Kim K (2022) Polarization manipulation of giant photonic spin Hall effect using wave-guiding effect. J Appl Phys 132:053102. https://doi.org/10.1063/5.0100554
3. Bliokh KY, Rodríguez-Fortuño FJ, Nori F, Zayats AV (2015) Spin–orbit interactions of light. Nat Photonics 9:796–808
4. Bliokh KY, Nori F (2015) Transverse and longitudinal angular momenta of light. Phys Rep 592:1–38
5. Zhou X, Ling X, Luo H, Wen S (2012) Identifying graphene layers via spin Hall effect of light. Appl Phys Lett 101:251602
6. Ling X, Zhou X, Huang K, Liu Y, Qiu C-W, Luo H, Wen S (2017) Recent advances in the spin Hall effect of light. Rep Prog Phys 80:066401
7. Qi S, Da H, Yan X (2023) Topological edge state-induced enhancement of photonic spin Hall effect in a heterostructure with monolayer graphene. J Appl Phys 134:013102
8. Hosten O, Kwiat P (2008) Observation of the spin Hall effect of light via weak measurements. Science 319:787–790
9. Fedorov FI (2013) To the theory of total reflection. J Opt 15:014002. https://doi.org/10.1088/2040-8978/15/1/014002
10. Imbert C (1972) Calculation and experimental proof of the transverse shift induced by total internal reflection of a circularly polarized light beam. Physical Review D 5:787
11. Onoda M, Murakami S, Nagaosa N (2004) Hall effect of light. Phys Rev Lett 93:083901
12. Ali R (2022) Chirality-assisted spin Hall effect of light in the vicinity of the quasi-antidual symmetry mode of a chiral sphere. Phys Rev A 106:063508
13. Zhou X, Xiao Z, Luo H, Wen S (2012) Experimental observation of the spin Hall effect of light on a nanometal film via weak measurements. Phys Rev A 85:043809
14. Ren J, Li Y, Lin Y, Qin Y, Wu R, Yang J, Xiao Y-F, Yang H, Gong Q (2012) Spin Hall effect of light reflected from a magnetic thin film. Appl Phys Lett 101:171103
15. Zhang W, Wang Y, Chen S, Wen S, Luo H (2022) Photonic spin Hall effect in twisted few-layer anisotropic two-dimensional atomic crystals. Phys Rev A 105:043507
16. Kim M, Lee D, Yang Y, Kim Y, Rho J (2022) Reaching the highest efficiency of spin Hall effect of light in the near-infrared using all-dielectric metasurfaces. Nat Commun 13:1–7
17. Yin X, Ye Z, Rho J, Wang Y, Zhang X (2013) Photonic spin Hall effect at metasurfaces. Science 339:1405–1407
18. Xia J, Chen Y, Xiang Y (2021) Enhanced spin Hall effect due to the redshift gaps of photonic hypercrystals. Opt Express 29:12160–12168. https://doi.org/10.1364/OE.420907
19. Kong L-J, Wang X-L, Li S-M, Li Y, Chen J, Gu B, Wang H-T (2012) Spin Hall effect of reflected light from an air-glass interface around the Brewster's angle. Appl Phys Lett 100:071109
20. Zhou X, Ling X (2016) Enhanced photonic spin Hall effect due to surface plasmon resonance. IEEE Photonics J 8:1–8
21. Yu X, Wang X, Li Z, Zhao L, Zhou F, Qu J, Song J (2021) Spin Hall effect of light based on a surface plasmonic platform. Nanophotonics 10:3031–3048
22. Luo H, Ling X, Zhou X, Shu W, Wen S, Fan D (2011) Enhancing or suppressing the spin Hall effect of light in layered nanostructures. Phys Rev A 84:033801
23. Tan X-J, Zhu X-S (2016) Enhancing photonic spin Hall effect via long-range surface plasmon resonance. Opt Lett 41:2478–2481
24. Cheng J, Xiang Y, Xu J, Liu S, Dong P (2022) Highly sensitive refractive index sensing based on photonic spin Hall effect and its application on cancer detection. IEEE Sens J 22:12754–12760
25. Zhu T, Lou Y, Zhou Y, Zhang J, Huang J, Li Y, Luo H, Wen S, Zhu S, Gong Q (2019) Generalized spatial differentiation from the spin Hall effect of light and its application in image processing of edge detection. Phys Rev Appl 11:034043
26. Baitha MN, Kim K (2022) Polarization switchable enhanced photonic spin Hall effect for optical switch and filters. IEEE Photonics Technol Lett 34:1329–1332
27. Ahlawat L, Kishor K, Sinha RK (2024) Photonic spin Hall effect-based ultra-sensitive refractive index sensor for haemoglobin sensing applications. Opt Laser Technol 170:110183
28. Kim M, Lee D, Rho J (2022) Incident-polarization-independent spin Hall effect of light reaching half beam waist. Laser Photonics Rev 16:2100510
29. Kim M, Lee D, Rho J (2021) Spin Hall effect under arbitrarily polarized or unpolarized light. Laser Photonics Rev 15:2100138
30. Baitha MN, Kim K (2022) All angle polarization-independent photonic spin Hall effect. Opt Laser Technol 156:108458
31. Maradudin AA, Sambles JR, Barnes WL (2014) Modern plasmonics. Elsevier
32. Jing J-Y, Wang Q, Zhao W-M, Wang B-T (2019) Long-range surface plasmon resonance and its sensing applications: a review. Opt Lasers Eng 112:103–118
33. Peatross J, Ware M (2011) Physics of light and optics. Brigham Young University, Department of Physics
34. Reather H (1988) Surface plasmons on smooth and rough surfaces and on gratings. Springer Tracts Modern Phys 111:1–3
35. Abd El-Fattah ZM, Mkhitaryan V, Brede J, Fernández L, Li C, Guo Q, Ghosh A, Echarri AR, Naveh D, Xia F (2019) Plasmonics in atomically thin crystalline silver films. ACS Nano 13:7771–7779
36. Ilchenko SG, Lymarenko RA, Taranenko VB (2016) Metal-multilayer-dielectric structure for enhancement of s-and p-polarized evanescent waves. Nanoscale Res Lett 11:1–3
37. Ilchenko SG, Lymarenko RA, Taranenko VB (2017) Using metal-multilayer-dielectric structure to increase sensitivity of surface plasmon resonance sensor. Nanoscale Res Lett 12:295. https://doi.org/10.1186/s11671-017-2073-1
38. Nesnidal RC, Walker TG (1996) Multilayer dielectric structure for enhancement of evanescent waves. Appl Opt 35:2226–2229
39. Qin Z, Liu Q, Yue C, Lang Y (2019) Modified model of photonic spin Hall effect of Gaussian beam reflected from a dielectric interface. Appl Phys Express 12:062008
40. Maniyara RA, Rodrigo D, Yu R, Canet-Ferrer J, Ghosh DS, Yongsunthon R, Baker DE, Rezikyan A, García de Abajo FJ, Pruneri V (2019) Tunable plasmons in ultrathin metal films. Nat Photonics 13:328–333
41. Garcia de Abajo FJ (2014) Graphene plasmonics: challenges and opportunities. ACS Photonics 1:135–152
42. Manjavacas A, García de Abajo F (2014) Tunable plasmons in atomically thin gold nanodisks. Nat Commun 5:1–7
43. Nagpal P, Lindquist NC, Oh S-H, Norris DJ (2009) Ultrasmooth patterned metals for plasmonics and metamaterials. Science 325:594–597
44. Martinez-Cercos D, Paulillo B, Maniyara RA, Rezikyan A, Bhattacharyya I, Mazumder P, Pruneri V (2021) Ultrathin metals on a transparent seed and application to infrared reflectors. ACS Appl Mater Interfaces 13:46990–46997
45. Wang F, Fu Y, Xiao S, Skallerud BH, Liu S, Luo S, Kristiansen H, He J, Zhang Z (2023) Thickness mediated morphology evolution

in sub-10-nm metal film deposition: implications for nondestructive testing. ACS Applied Nano Materials 6:11491–11499
46. Xiang Y, Jiang X, You Q, Guo J, Dai X (2017) Enhanced spin Hall effect of reflected light with guided-wave surface plasmon resonance. Photonics Res 5:467–472